Journal of Controlled Release 329 (2021) 907–918

Contents lists available at ScienceDirect

Journal of Controlled Release

journal homepage: www.elsevier.com/locate/jconrel

High resolution photopolymer for 3D printing of personalised microneedle for transdermal delivery of anti-wrinkle small peptide

Seng Han Lim [a], Himanshu Kathuria [a], Muhd Hafiz Bin Amir [a], Xiyuan Zhang [b], Hien T. T. Duong [b], Paul Chi-Lui Ho [a], Lifeng Kang [b,*]

[a] Department of Pharmacy, National University of Singapore, 18 Science Drive 4, Block S4A, Level 3, Singapore 117543, Republic of Singapore
[b] School of Pharmacy, Faculty of Medicine and Health, University of Sydney, Pharmacy and Bank Building A15, Science Road, NSW 2006, Australia

ARTICLE INFO

Keywords:
3D printing
Microneedle
Transdermal drug delivery
Small peptide
Photopolymer

ABSTRACT

Acetyl-hexapeptide 3 (AHP-3) has good efficacy and safety profile as an anti-wrinkle small peptide. However, its skin permeation is poor due to its hydrophilicity and large molecular weight. 3D printing of personalised microneedles (MN), that contour to the skin surface, offers an attractive alternative for delivery for AHP-3. However, commercially available photocurable resin for 3D printing are not suitable for fabrication of drug loaded delivery systems. In this study, two liquid monomers, namely, polyethylene glycol diacrylate (PEGDA) and vinyl pyrrolidone (VP), were investigated at various proportions, for critical parameters such as mechanical strength of final polymer, rate of polymerisation, rate of swelling of final polymer, 3D printing resolution and safety profile of final polymer. The optimal resin, based on the above parameters, was that of ratio 7 VP: 3 PEGDA in weight. Drug loading into the optimal resin demonstrated that AHP-3 remained stable throughout the fabrication process and there was no effect on the physical properties of final polymer. Using a 3D scanned face model, a personalised MN patch was designed using computer aided design (CAD) software and subsequently fabricated using a Digital Light Processing (DLP) 3D printer, with the optimal resin. In vitro characterisation of fabricated MN patch demonstrated the ability to penetrate human cadaver dermatomed skin and the MN remained intact after compression. The final polymer also had minimal cytotoxicity to human dermal fibroblast. Therefore, personalised MN patch fabricated using the photopolymer can potentially be a novel approach to augment transdermal delivery of AHP-3 for effective wrinkle management.

1. Introduction

Wrinkles, the first sign of ageing, are often presenting as folds or creases in the skin. One of the most vulnerable area to wrinkle formation is the periorbital region [1,2]. In scenarios when an individual becomes too paranoid or troubled by these facial wrinkles, psychosocial impacts such as reduced occupational functioning and lowered self-esteem may occur [3]. Therefore, effective treatment for wrinkles is essential to improve the quality of life of these individuals.

By far, Botox has been one of the most effective and commonly injected substances to reduce wrinkles in the United States with up to 1.5 million injections in 2017 [4]. However, it has been questioned for its safety in human, due to its toxicity and therefore, its use has been under strict control [5]. Acetyl hexapeptide-3 (AHP-3), or Argireline®, is a topical Botox-mimetic agent that inhibits the release of acetylcholine and reduces the repeated contractions of intrinsic muscles regulating facial expression, thereby decreasing hyperkinetic facial lines or expression wrinkles [6–8]. It is desirable for wrinkle management due to its low toxicity ($\geq$2000 mgkg^{-1}) and non-invasiveness, as compared to the Botox (20 ngkg^{-1}) which has to be injected directly into the facial muscle [6]. Furthermore, AHP-3 has been found to be an effective anti-wrinkle agent, with ~49% improvement after 4 weeks of twice daily treatment [6,9,10]. However, its permeation through skin is poor due to its high molecular weight (889 Da) and low LogP value (−6.3) [8]. According to Kraeling et al., only 0.01% of AHP-3 permeated through the stratum corneum and reached the viable epidermis after topical application [11]. A significant amount of the peptide remained on the skin surface, leading to wastage and possibly reduced efficacy. Several research groups have attempted to improve the transdermal delivery of AHP-3 through formulation approach [11–13] or molecular modification approach [14], but have only achieved modest improvement.

Microneedles (MN) is a minimally invasive technique used to create

* Corresponding author.
E-mail address: lifeng.kang@sydney.edu.au (L. Kang).

https://doi.org/10.1016/j.jconrel.2020.10.021
Received 22 October 2019; Received in revised form 4 October 2020; Accepted 11 October 2020
Available online 15 October 2020

micro pores within the stratum corneum or epidermis to enhance the delivery of chemicals and macromolecules, especially the large and hydrophilic peptides such as AHP-3, across the skin [15–19]. Unlike hypodermic needles, the small size of MN avoids the nerve endings present only in the dermis or deeper and can therefore, provide a pain free delivery of drugs. This makes MN ideal for improving patient adherence and can be self-administered by the patient.

Current MN arrays are superimposed onto flat planar patches to facilitate their insertion into the skin [20]. However, the human skin is undulating and personalised due to mainly the body anatomy and also variations in skin elasticity or the amount of hair on the skin [20]. On such curved surfaces around the bones, MN arrays fabricated on a flat patch are not completely inserted and large amount of loaded materials are not delivered [20]. Furthermore, traditional flat MN arrays are subjected to the "bed of nails" effect where the force on each MN is equally distributed across the array. This results in the inability of all MN to overcome the elasticity of the epidermis and punctures the skin [21].

To minimise this variation in the skin, most MN arrays are spread only over small areas. As a result, the amount of drugs loaded onto the small area of MN arrays is limited and MN usage is largely restricted to potent drugs such as vaccines [15,22–24]. To this issue, several research groups have created flexible [25–27], curved [28] or personalised MN patches [29,30]. Out of these, personalised MN patches (PMNP) using vat polymerisation 3D printing appears to be the most promising alternative, due to its single step ease of fabrication and its ability to incorporate human 3D scans to achieve a true PMNP to account for all contours of the skin.

However, the limited number of commercially available photocurable resin to produce biocompatible products is often perceived as a key challenge for vat polymerisation 3D printers [31]. Traditional resins are also known to be generally poor in their mechanical strength [31]. In addition, not all resins allow drug loading of any type nor do they release these drugs after polymerisation. Therefore, there is a need for development of a high-resolution biocompatible resin with good mechanical strength and has the potential for drug release after being loaded with drug. Here, in this study, we explored the potential of digital light processing (DLP) 3D printer for the fabrication of PMNP to deliver an anti-wrinkle small peptide. Polyethylene glycol diacrylate (PEGDA, MW 700 Da) and vinyl pyrrolidone (VP) are both photoreactive monomers and present as liquid at room temperature, therefore making them suitable candidates for DLP 3D printing. In addition, both monomers polymerise into biocompatible polymers which have been used in pharmaceutical applications [32,33].

Using various proportions of PEGDA and VP, we obtained an optimal resin based on the parameters which were critical for an ideal 3D printing material. These parameters include mechanical properties of the final polymer, safety profile of final polymer, 3D printing resolution, rate of drug release and rate of polymerisation. Fig. 1 depicts a schematic representation of the copolymerization of PEGDA and NVP induced by UV light (405 nm). Finally, with the optimal resin, a PMNP based on a scanned human periorbital region was fabricated and tested for its efficacy and safety.

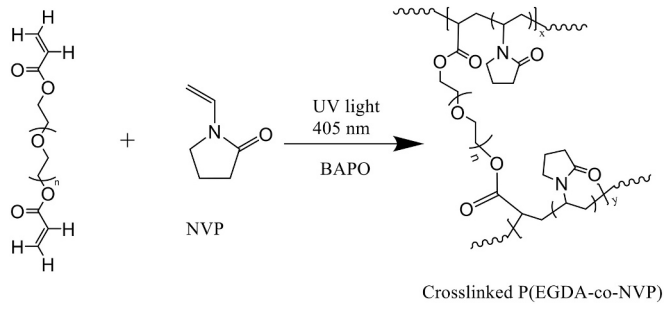

Fig. 1. Schematic representation of the copolymerization of PEGDA and NVP induced by UV light (405 nm).

2. Material and methods

2.1. Material

AHP-3 was received from Kaijie Peptide Company (Sichuan, China). Trypan blue, phosphate buffered saline (PBS), polyethylene glycol diacrylate (MW: 700 Da), 4,4′-Azobis(4-cyanovaleric acid (ABCV); Phenylbis (2,4,6-trimethylbenzoyl) phosphine oxide (BAPO); 2-Hydroxy-4′-(2-hydroxyethoxy)-2-methylpropiophenone (HHEMP) were purchased from Sigma-Aldrich (Merck KGaA, Darmstadt, Germany). Vinyl pyrrolidone (VP) and deuterated dimethyl sulfoxide (DMSO) was purchased from Merck (Merck KGaA, Darmstadt, Germany). PrestoBlue® was obtained from Invitrogen (Carlsbad, CA, USA). Culture media consisted of Dulbecco's Modified Eagle Medium (DMEM) (Invitrogen) supplemented with 10% of fetal bovine serum (FBS) (Invitrogen) and 1% of 10,000 U ml^{-1} penicillin and 10 mg ml^{-1} streptomycin (PS) (PAN-Biotech GmbH, Germany). All mentions of water refer to deionized, grade 1 water filtered from a laboratory water purification system (Adrona Crystal, Latvia), unless otherwise stated. Polydimethylsiloxane (PDMS) (Sylgard 184 Silicone Elastomer Kit) was obtained from Dow Corning (Midland, MI, USA). 3DM-Castable resin was purchased from 3D-Materials SASU (Feldkirch, France). Human cadaver dermatomed skin was obtained from Science Care (Arizona, USA). The skin tissues were excised from a 66 years old Caucasian female and the use of these skin tissues were approved by NUS Institutional Review Board (IRB). All other reagents were of analytical grade.

3. Method

3.1. Choice / concentration of suitable photoinitiator for use with digital light processing (DLP) 3D printer

DLP 3D printer of choice is Pico 2 HD (Asiga, Sydney, Australia), which has a working UV–Vis wavelength of 405 nm. To determine the suitable photoinitiator for DLP 3D printer, UV/VIS-spectra of the photoinitiators were measured with a UV/VIS-spectrometer (U-1800, Hitachi, Japan) using a 1% *w/v* solution in methanol. This was repeated with various concentrations (0.01, 0.1, 0.5, 1, 2% *w/v*) of photoinitiators.

3.2. Preparation of various composition of photopolymer

The photoinitiator (BAPO) concentration was kept at 0.5% *w*/w. Between VP and PEGDA, a total of 5 different photopolymer combinations was prepared in the ratios of 10:0, 7:3, 5:5, 3:7, 0:10. Each of the monomer liquid was weighed out accurately and mixed with each other. To the resultant resin, accurately weighed amount of BAPO was added to it and vortexed till complete dissolution.

3.3. Rheological measurement of polymerisation curve and rate of reaction

Storage modulus of photopolymer resin was measured throughout its polymerisation reaction with the use of a rheometer (M302, Anton Paar GmbH, Graz, Austria), coupled with UV light source (Omnicure Series 1500, Excelitas Technologies Corporation, MA, USA) for photo polymerisation reaction. Throughout the entire measurement, a disposable parallel plate of 8 mm diameter (D-PP08) was used at a shear strain of 0.001, frequency of 1 Hz and temperature of 25 °C. The first 2 mins was used to stabilise the system and measurements were taken at 10 s interval. Beyond 120 s, UV light was turned on and measurements were taken at 1 s interval. The measurement lasted for a total of 42 min per sample. Time taken to reach 90% of maximum storage modulus was calculated to determine the reactivity rate of each photopolymer

combination. The shorter the time taken, the higher the reactivity rate, making it more suitable for use in 3D printing.

3.4. Fabrication of polymer using UV photo polymerisation for PDMS moulded cylinders

All polymer samples of various photopolymer combination were fabricated with the use of PDMS moulds of various dimensions. PDMS moulds were fabricated through the following steps. Briefly, a mixture of silicone elastomer base and silicone elastomer curing agent in 9:1 ratio by weight was poured into the respective containers with the desired dimensions. Subsequently, the mixture was degassed in a vacuum chamber prior to heat curing at 70 °C for 2 h to obtain the PDMS moulds. Once the prepolymer solution were added to the mould, the entire PDMS mould is transferred into a UV post cure chamber (Post cure chamber, Asiga, Sydney, Australia) and photopolymerised for 20 min. Each cylindrical rod was then removed from the PDMS moulds and soaked in 70%*v*/v ethanol for 30 s, followed by water for 30 s and finally post cured in the same UV post cure chamber for an additional 30 min, before being used for any testing.

3.5. Force displacement curve / calculated young's modulus for PDMS moulded cylinders

Polydimethylsiloxane (PDMS) moulds with cylindrical holes measuring 11 mm in diameter, 8 mm in height, were prepared in advance. 760 μL of each photopolymer combinations were added to the PDMS moulds and photopolymerised as per Section 2.5. Mechanical strength was conducted using these homogenously shaped cylinders to prevent any confounding due to other random shapes of the microneedles. A force gauge (JSV H1000, Algol Instrument Co. Ltd., Taiwan) was used to measure the displacement curve of the cylindrical rods for each photopolymer combination. Using the linear portion of a force-displacement curve, a stress-strain curve was calculated, and its gradient was determined as the Young's Modulus of the photopolymer combination.

3.6. Swelling test for PDMS moulded cylinders

PDMS moulds with cylindrical holes measuring 4 mm in diameter, 4 mm in height, were prepared in advance. 40 μL of each photopolymer combination was added to the PDMS mould and photopolymerised as per Section 2.6. Swelling test was conducted using these homogenously shaped cylinders to prevent any confounding due to other random shapes of the microneedles. Both PEGDA and VP are known to polymerise into hydrophilic polymers which absorb water. The rate of swelling or volume expansion of the polymer during contact with PBS was observed and used as a surrogate for rate of drug release. The weight of each polymer ranging from 40 to 50 mg was noted on a weighing machine before it was immersed in 5 mL of PBS. At time points of 0.25, 0.5, 1, 2, 4, 6 and 48 h, polymer was removed from PBS and dried with lint free tissue Kimwipes™ before being weighed on the same weighing machine.

3.7. Monomer conversion ratio for PDMS moulded cylinders

2 pieces of flat, circular PDMS were used as moulds in this case. 200 μL of each photopolymer combination was added to the top of 1 circular PDMS. Slowly, the second piece of PDMS was stacked on top. Any excess photopolymer that overflowed out of the 2 PDMS were wiped away. The photopolymer was then photopolymerised as per Section 2.5. The thin film of polymer is then cut into small pieces and ground down to fine particles using a pestle and mortar. 20 mg of this polymer was mixed with 1.2 mL of deuterated DMSO containing 4 mg of 1,3,5 trioxane as internal standard (IS) and left to stand for 24 h at room temperature (to extract any residual monomers). At the end of 24 h, the polymer extract was centrifuged and 600 uL of extract was removed for analysis via ^{1}H NMR. Similarly, 10 mg of prepolymer photopolymer combination was mixed with 600 μL of deuterated DMSO containing 2 mg of 1,3,5 trioxane as an internal standard and analysed via ^{1}H NMR immediately. ^{1}H NMR was used to determine the amount of double bonds (characteristic of monomers) in the prepolymer photopolymer combination and the final extract from the synthesised polymer. Monomer conversion ratio was calculated based on the below formula:

$$\text{Percentage of Monomer Conversion} = \left(1 - \frac{\text{Amount of Residual monomer}}{\text{Amount of Initial monomer}}\right) \times 100\%$$

3.8. Cytotoxicity assay for PDMS moulded cylinders

The test for biocompatibility was designed based on EN ISO 10993-12:2012 guidelines. PDMS moulds with cylindrical holes measuring 2 mm in radius, 4 mm in height, were prepared in advance. Cylindrical rods with a total surface area of 4.5 cm^2 were added to 1.5 mL (3: 1 surface area to volume ratio) of complete DMEM culture media supplemented with 10% fetal bovine serum and 1% penicillin/streptomycin, incubated at 37 °C with agitation, for a duration of 24 h. Human dermal fibroblast (HDF) and human adult low calcium high temperature (HaCaT) cells were used to assess the toxicity of the polymer extract. Cells were grown in complete DMEM culture media supplemented with 10% FBS and 1% penicillin/streptomycin. Five thousand cells were plated into 96-well microtiter plates in 200 μL of culture medium. After 24 h of incubation at 37 °C and 5% CO_2, all culture medium was removed and replaced with 200 μL of polymer extract for each well. The negative control consisted of wells containing 200 μL of fresh culture medium. The plates were incubated at 37 °C and 5% CO_2 for 24 h. At the end of 24 h, one batch of cells were used for PrestoBlue® analysis. For the other batch, polymer extracts were replaced with 200 μL of fresh culture media and incubated for an additional 48 h. At the respective time points, all media in the wells were replaced with 90 μL of sterile PBS and 10 μL of PrestoBlue® cell viability reagent. The 96-well plate was then incubated for 2 h under the same incubation conditions stated above. Finally, the absorbance of the wells was analysed with an absorbance plate reader (SpectraMax® 190, Sunnyvale, CA, USA) at a wavelength of 570 nm with a reference wavelength of 600 nm. This utilizes the reducing power of metabolically active cells to reduce resazurin to resorufin, with wavelengths of maximum absorbance of 600 nm and 570 nm, respectively. A higher absorbance readout of 570 nm over 600 nm indicates the presence of viable cells. The 570 nm absorbance readings will be subtracted from the 600 nm readings for all treated wells to obtain the normalized absorbance. The normalized background absorbance of resorufin was determined from the blanks and subtracted from the normalized absorbance of the experimental and standard reference wells to obtain the corrected absorbance. Subsequently, the corrected absorbance of the experimental wells was expressed as a percentage of that of the control to determine the relative cell viability. The entire procedure was later repeated for a 3D printed cube to evaluate the safety of PMNP printed using the 3D printing and its set of parameters.

3.9. Drug release & recovery study for AHP-3 loaded cylinders

PDMS moulds with cylindrical holes measuring 8 mm in diameter, 4 mm in height, were prepared in advance. 165 μL of each photopolymer combination loaded with either 0.5%*w*/w or 0.1% w/w of AHP-3 was added to the PDMS mould and photopolymerised as described in Section 2.6. Each fabricated cylinder was placed in 5 mL of PBS, maintained at 32 °C for up to 48 h, to determine the release profiles of AHP-3

embedded in the various photopolymer combinations. Sampling of the dissolution media was taken at 5 min, 15 min, 1 h, 2 h, 4 h, 6 h, 8 h, 12 h, 24 h and 48 h and fresh PBS was replaced after each sampling. At the end of 48 h, the remaining cylinder was homogenized at 500 rpm for 5 min using a High Shear Homogenizer (PT3100D, Polytron, Indiana, United States). Subsequently, all samples were centrifuged and the supernatant was analysed to determine the quantity of AHP-3 present.

3.10. Effect of AHP-3 Loading on physical properties of selected photopolymer resin

AHP-3 (0.5% *w*/w) was added to the optimised photopolymer combination. To create a uniform suspension, the resultant mixture was sonicated for 2 periods of 30 s each, with an interval of 1 min. This uniform suspension was used for rheological testing and determination of Young's Modulus as per described in Sections 2.5 and 2.7, respectively.

3.11. Drug analysis

The quantity of AHP-3 was determined using Shimadzu LC-20AD High Performance Liquid Chromatography (HPLC) machine with SDP-M20A UV detector. The column used was an Agilent Zorbax Eclipse Plus C18 column (3 mm × 150 mm × 5 μm, 95 Å). The mobile phase consisted of mobile phase A (0.1% *v*/v trifluoroacetic acid in water) and mobile phase B (0.1% v/v trifluoroacetic acid in acetonitrile) with an isocratic elution program and ratios of solvents A:B of 9:1. The flow rate was set at 1 mL min^{-1}. The injection volume was 20 μL for each sampling and UV detection was executed at a wavelength of 215 nm. A calibration curve was plotted using the respective standard solutions from 1 ppm to 500 ppm.

3.12. 3D scan of human volunteer

3D scanning of the face of a human volunteer (30-year-old, Chinese, Male) was performed with a commercial scanner (Artec Eva, Artec3D, Luxembourg) at a distance of ~50 cm away from the human volunteer in accordance with the manufacturer's recommendations. The 3D scanner was panned 360° around the head of the volunteer to capture a 3D image that was exported directly to the corresponding software Artec Studio 11 (Artec3D, Luxembourg) for processing. The final CAD model of the human volunteer face was saved and subsequently processed using a suite of programme including Fusion 360 (Autodesk® Inc., San Rafael, CA, USA), Remake (Autodesk® Inc., San Rafael, CA, USA) to convert it into a solid model which can be imported into Solidworks® 2016 (Dassault Systemes, France).

3.13. Design and fabrication of PMNP

The human face CAD model was processed using Solidworks® 2016 (Dassault Systemes, France). A personalised eye patch was designed to fit snugly to the contours and dimensions of the face CAD model. Subsequently, arrays of MNs were created on the patch's inner contoured surface. The MNs were designed to have 400 μm base diameter, 800 μm center-to-center spacing. The MN height was set at 800 μm and with a tip diameter of 100 μm, with a total of 927 MN. The completed CAD model was exported as STL file and opened in the Asiga Composer V 1.1.7 software for optimisation of the print parameters such as exposure time, lift speed etc. Briefly, the DLP 3D printer function based on the principles of vat polymerisation. Once the build platform is lowered into the resin, the DLP projector projects a 2D image, as determined by the individual image slices, and polymerises a thin layer of liquid resin into a solid. The build platform then separates from the resin container to allow fresh resin to flow in. This process repeats, until the entire object is printed. After the patch was printed, it was soaked in 70% *v*/v ethanol in deionized water for 30 s, followed by pure deionized water for 30 s. The printed microneedle patch was finally post cured in the Asiga UV post cure chamber for an additional 30 min, before being used for any testing.

3.14. Mechanical strength testing for PMNP

The fabricated PMNP was first photographed with Nikon SMZ-25 stereomicroscope (Nikon, Japan) and Nikon imaging software (NIS-Element Analysis D 4.20.00) to obtain 'before' images. Next, the PMNP was compressed, using a thumb force, against a personalised acrylonitrile butadiene styrene (ABS) substrate corresponding to the PMNP for 30 s. The personalised ABS substrate was fabricated via Fused Deposition Modelling 3D printer (CEL Robox®, England, UK). Subsequently, the PMNP was photographed with the same stereomicroscope to obtain 'after' images. The 'before' & 'after' images were then visually compared to identify MN fractures and determine the percentage of intact MNs. A triplicate was conducted for this test.

3.15. Preparation of human cadaver skin prior to use

Human cadaver dermatomed skin, after excision, were stored in −80 °C freezer until use. The use of cadaver human skin has been reviewed by the National University of Singapore Institutional Review Board and subsequently exempted because the cadaveric tissues used in this study were without identifiable private information. Skin samples were hydrated in water prior to use. The skin was measured for the electrical resistance using an electrical resistance meter (LCR-916, GW Instek, Good Will Instrument Co. Ltd., Taiwan). Based on internal lab standards, human cadaver dermatomed skin is required to have a minimum electrical resistance of 1 kV, at 1 kHz in 1 X PBS solution, before it is considered as intact with a complete skin barrier. Any skin samples with electrical resistance below 1 kV were not used.

3.16. Skin penetration efficiency testing for PMNP

Personalised PDMS substrate corresponding to the PMNP, which mimics full-thickness skin, was prepared in advance [17,29,34]. Human cadaver dermatomed skin was laid stretched over the personalised PDMS substrate with epidermis facing up and the PMNP was compressed onto the skin using a thumb (~20 N) in a slow rotational motion for 30 s. Excess trypan blue dye was added onto the skin and left on for 10 min. At the end of 10 min, trypan blue was wiped off using 70%*v*/v ethanol. Subsequently, the stained skin sample was visualized using the Nikon SMZ-25 stereomicroscope to demonstrate the presence of skin penetration. The blue stained dots represent the punctured pores due to the selective staining nature of trypan blue.

3.17. In vitro cellular cytotoxicity of 3D printed cubes

To evaluate any cytotoxicity of the optimal photopolymer and the 3D printing process, 3D printed cubes were used instead of PDMS moulded cubes. The same procedures were performed as in Section 2.10. The only exception is that 6 cubes of 5 mm length were used for extraction of residual monomers in 3 mL of complete culture media.

3.18. Statistical / data analysis

All data were collated and prepared using GraphPad Prism 6 (GraphPad Software Inc., CA, USA) for any graphical outputs. All experiments were conducted in triplicates and the results presented as mean ± standard deviation. Statistical analysis was performed by one-way analysis of variance followed by Tukey post hoc test or Student Independent Samples *t*-test, using IBM SPSS Statistics 21.0 (IBM, New York, USA). A probability value of $p < 0.05$ was considered statistically significant.

4. Results

4.1. Choice / concentration of suitable photoinitiator for use with digital light processing (DLP) 3D printer

Based on the UV / Vis absorbance spectrum between 200 nm to 700 nm of different common photoinitiators as illustrated in Fig. 2A, only BAPO demonstrated significant absorbance at 405 nm. Subsequently, various concentration of BAPO were tested for its absorbance at 405 nm, as illustrated in Fig. 2B. As the concentration increased, the absorbance of BAPO at 405 nm increased until a point of saturation at 0.5% *w*/w BAPO and beyond. Any concentration above 0.5% w/w BAPO did not provide any additional absorbance at 405 nm. Therefore, the most suitable type and concentration of photoinitiator is 0.5% w/w BAPO.

4.2. Rheological measurement of polymerisation curve and rate of reaction

Five different photopolymer combinations were tested for their change in storage modulus with time during photo polymerisation. In general, the higher the percentage of PEGDA, the faster is the time to 90% polymerised, as illustrated in Fig. 3B. For instance, a 30% addition of PEGDA, shortened the time to 90% polymerised by over 400 s (comparing 100% VP to 70%VP, 30% PEGDA). Commercial castable resin which has been demonstrated in previous literature for MN fabrication, was used as a comparison [29]. Only photopolymer combinations with 50% or more PEGDA has a faster time to 90% polymerised as compared to castable resin. On the other hand, the higher the percentage of VP, the higher the storage modulus, which may be indicative of its mechanical strength, as illustrated in Fig. 3A. Photopolymer combinations containing 50% or more PEGDA demonstrated a detectable 2 stage polymerisation as per seen in the 2 separate plateaus in storage modulus for 50:50% VP:PEGDA and 70:30% VP:PEGDA. This may be due to the difference in reactivity of acrylate group versus that of vinyl group in the tendency for polymerisation.

4.3. Young's modulus

Similarly, 5 different photopolymer combinations were tested for their mechanical strength by measuring their force-displacement curve and calculating their respective Young's Modulus. As illustrated in Fig. 4A, the higher the percentage of VP, the steeper is the force-displacement curve, which indicates a higher mechanical strength. However, it was also demonstrated that 100% VP may be brittle in nature, as seen in the breakage of force-displacement curve midway. Similarly, for 70:30% VP:PEGDA, there was a small plateau in the force-displacement curve midway, possibly indicating a small breakage which was still able to maintain the overall force applied onto it. Young's Modulus, is the measurement of the stiffness of a material. As illustrated in Fig. 4B, a higher percentage of VP demonstrated a higher Young's Modulus and therefore, more suitable for use in the fabrication of MN which require high mechanical strength. Commercial castable resin which has been demonstrated in previous literature to be of sufficient strength for MN skin penetration, was used as a comparison [29]. All combinations of photopolymers have a higher Young's Modulus as compared to castable resin, with the exception of 30:70% PEGDA:VP.

4.4. Swelling test in PBS

All 5 different photopolymer combinations were fabricated as cylindrical rods and immersed in PBS to determine the change in weight of polymer due to swelling over time. A higher change in weight indicates a higher release rate of drugs embedded within the polymer. A faster change in weight indicates a faster release rate of drugs embedded within the polymer. As illustrated in Fig. 5A, 100% VP completely dissolved in PBS and therefore has no measurable change in weight. For the remaining 4 combinations, polymers with a higher percentage of VP demonstrated a higher and faster changing rate in weight or swelling rate.

4.5. Determination of monomer conversion

To find the monomer conversion rate, ^{1}H NMR spectroscopy was employed to monitor the consumption of VP and PEGDA individually through their non-overlapping vinylic proton signals. As shown in Fig. S1 and S2, the chemical shift from 5.9–6.4 ppm was assigned to the protons of vinyl groups of PEDGA, while that at 6.9 ppm was assigned for the vinyl groups of VP. The analysis of the ^{1}H NMR spectra using the integration of vinylic proton signals of VP (6.9 ppm) and PEGDA (6.4 ppm) by comparing with the unchanged integration of the protons of

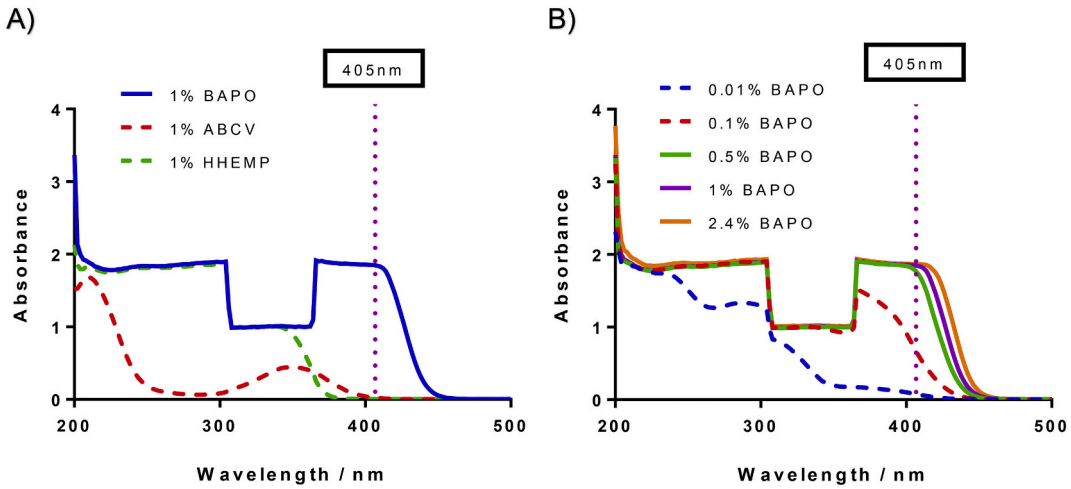

* BAPO: Phenylbis(2,4,6-trimethylbenzoyl)phosphine oxide; ABCV: 4,4′-Azobis(4-cyanovaleric acid); HHEMP: 2-Hydroxy-4′-(2-hydroxyethoxy)-2-methylpropiophenone

Fig. 2. UV absorbance graph for different type and concentration of photoinitiators. A) UV absorbance graph of 3 different common photoinitiators. Only BAPO has significant absorbance at a wavelength of 405 nm, making it suitable for use in DLP 3D printers that uses UV–Vis wavelength for fabrication. B) UV absorbance graph of various concentration of BAPO. Beyond 0.5% BAPO, there is no increment in absorbance at 405 nm. Therefore, 0.5% BAPO is a suitable concentration for use. The graphs comprise of a single representative set of data for each parameter.

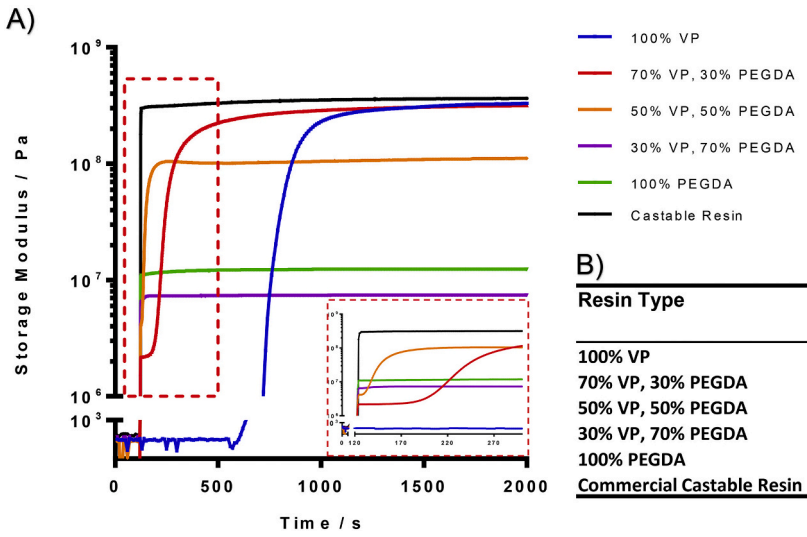

B)

Resin Type	Time to 90% polymerised / s Average (± S.D.)
100% VP	1340.0 (± 60.0)
70% VP, 30% PEGDA	930.7 (± 72.5)
50% VP, 50% PEGDA	151.7 (± 107.7)
30% VP, 70% PEGDA	13.3 (± 0.6)
100% PEGDA	23.7 (± 9.0)
Commercial Castable Resin	360.3 (± 90.2)

Fig. 3. Reactivity rate of various combination of VP and PEGDA. A) Polymerisation curve of different combination of VP and PEGDA. Generally, the greater the percentage of PEGDA, the higher the reactivity rate, making it more suitable for 3D printing. Appeared to have 2 stages of polymerisation, firstly, that of the quick reacting acrylate group, then subsequently, the slower vinyl group. Also, generally, the greater the PEGDA, the lower the storage modulus. B) Summary table for time to 90% polymerised. Generally, the greater the percentage of PEGDA, the faster it takes to reach 90% polymerisation. The experiment was performed in triplicates. However, the graph comprises only of a single representative set of data for each parameter.

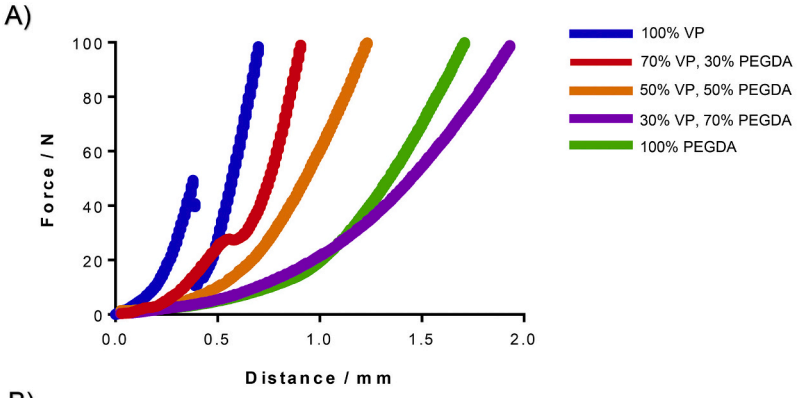

B)

Resin Type	Young's Modulus (MPa) Average	S.D.
100% VP	38.83	8.85
70% VP, 30% PEGDA	29.12	4.51
50% VP, 50% PEGDA	18.20	0.39
30% VP, 70% PEGDA	11.56	1.56
100% PEGDA	15.50	0.25
Commercial Castable Resin*	11.19	-

Fig. 4. Mechanical properties of polymer fabricated from the various combinations of VP and PEGDA. A) Force displacement curve. In general, the greater the percentage of VP, the steeper the force displacement curve and the greater the mechanical strength. However, while pure VP has good strength, it is also brittle, as illustrated by the break in force displacement curve. B) Summary table of the calculated Young's Modulus. In general, the greater the percentage of VP, the higher the Young's modulus. A comparison to the commercial castable resin was made. *Value obtained from material data sheet. The experiment was performed in triplicates. However, the graph comprises only of a single representative set of data for each parameter.

internal standard (5.1 ppm) results in the individual monomer conversion of both monomers after the polymerisation. Typically, a low monomer conversion ratio is equated to high residual monomers and this may be a cause for concern due to its potential cytotoxicity thus it is crucial to determine the amounts of unreacted monomers trapped in the copolymers.

As illustrated in Fig. 6A, the rate of consumption of VP is slightly lower than that of PEGDA. It is noted that all copolymers containing PEGDA and VP demonstrated a high monomer conversion ratio of over 90% for VP and nearly 100% for PEGDA, which may allow the polymer to exhibit its true physical properties and also reduce the cytotoxicity due to residual monomers. On the other hand, the monomer conversion for homo-polymerisation of VP (~82%) was lower than that of PEGDA (100%). It has been reported that the rate of homo-polymerisation of acrylate monomers was higher than that of VP at fixed concentration of monomers and initiators [35].

4.6. Cytotoxicity assay on human dermal cell lines

PrestoBlue® reagent, a resazurin-based solution, was used as an indicator of cell viability to compare the relative cell viability of dermal cell lines treated with extracts of the various photopolymer and those without. As illustrated by Fig. 6B, relative cell viabilities of ~85% or more was observed for both HDF and HaCaT keratinocytes for all polymer extracts, except for that of pure VP polymer. The high cytotoxicity of pure VP polymer extracts corresponded to the lower

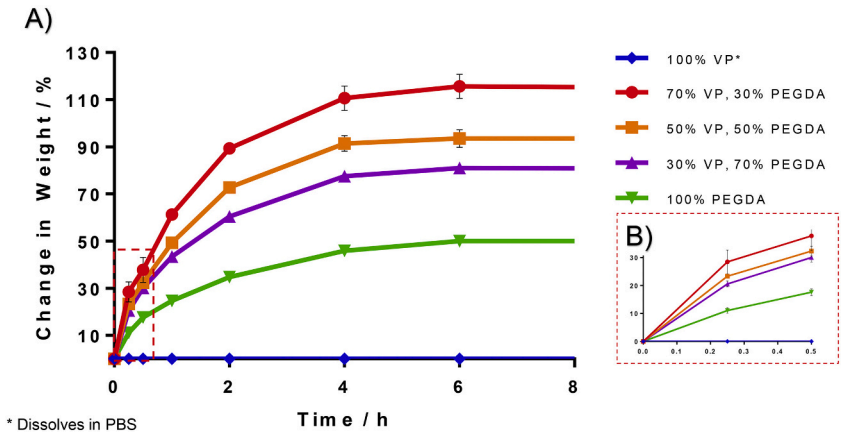

Fig. 5. Swelling test of polymer fabricated from various combinations of VP and PEGDA. A) Swelling test over 8 h. Swelling test was used as a surrogate for rate of drug release. A higher percentage of VP demonstrated a higher change in weight over 8 h. The greater the swelling, the higher the drug release. In general, the higher the percentage of VP, the faster the drug release. B) Zoomed in image of the first 0.5 h of swelling test. The experiment was performed in triplicates.

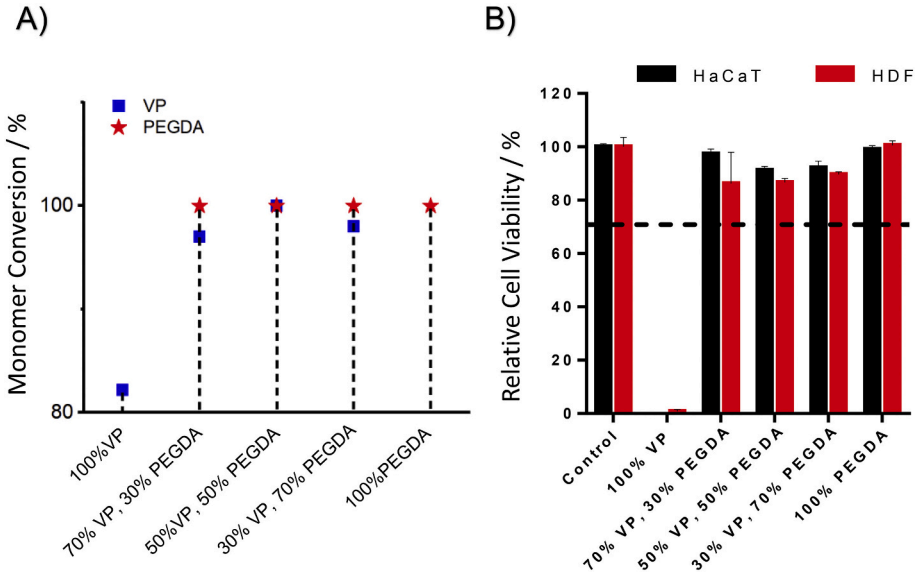

Fig. 6. Safety profiling of polymer fabricated from various combinations of VP and PEGDA. A) Monomer conversions of PEGDA and VP after copolymerisation. All polymers showed high monomer conversions (> 90%) for both VP and PEGDA, with the exception of pure VP polymer (80%). Typically, the higher the amount of residual monomer, the higher the toxicity. B) Cytotoxicity assay using human skin cells demonstrated safety of the fabricated polymer, with cell viability of all polymer extracts reaching more than 90% when the cells were given 48 h for recovery, after 24 h of exposure. However, cells exposed to polymer extracts from pure VP has almost zero survival. This corresponds to the lower monomer conversion ratio in pure VP. *HaCaT: Human adult low calcium high temperature keratinocytes; HDF: Human dermal fibroblast. The experiment was performed in triplicates. However, fig. A) comprises only of a single representative set of data for each parameter.

monomer conversion ratio as demonstrated in Fig. 6A. Therefore, the use of photopolymer combinations containing PEGDA may allow the fabrication of biocompatible products.

4.7. Drug release & recovery study of AHP-3 loaded cylinders

Cylinders of various photopolymer combinations were prepared with either 0.1% *w*/w or 0.5% w/w AHP-3. The drug release study conducted over a period of 48 h demonstrated a consistently highest rate and overall drug release for 50% VP, 50% PEGDA cylinders, amongst all other combinations of photopolymer, as shown in Fig. 7A and B. For the 50%VP, 50% PEGDA cylinders, by the end of 48 h, there was a complete release of AHP-3 for the 0.1% w/w loaded cylinders and an ~80% release of AHP-3 for the 0.5% w/w loaded cylinders. On the other hand, 100% PEGDA cylinders demonstrated consistently lowest rate and overall drug release amongst all other combinations of photopolymer. For the 100% PEGDA cylinders, by the end of 48 h, there was an ~35% release of AHP-3 for the 0.1% *w*/w loaded cylinders and a ~ 60% release of AHP-3 for the 0.5% w/w loaded cylinders. There were no clear differences between the release profiles of the other photopolymer combinations.

Finally, as illustrated by Fig. 7C, the representative HPLC chromatogram demonstrated no significant changes to the retention time of external standard AHP-3 dissolved in PBS versus the AHP-3 released from a 70% VP, 30% PEGDA photopolymer in PBS. Therefore, together with the drug release study it was demonstrated that the optimised resin and photo-polymerisation reaction has no significant effect on the stability of AHP-3.

4.8. Effect of AHP-3 loading into photopolymer resin

Based on the various optimisation test, the most optimal photopolymer resin was determined to be that of 70:30% VP:PEGDA. This was due to its high mechanical strength, rapid rate and extent of drug release and reasonable time taken to reach 90% polymerised. 0.5%*w*/w of AHP-3 was loaded into the optimised resin to form a uniform suspension. Cylindrical rods made from this optimised resin loaded with 0.5%w/w of AHP-3 has no significant difference in the Young's Modulus and time to 90% polymerised, as illustrated in Fig. 8A and B respectively. This demonstrated that AHP-3 does not affect the physical properties of the resin, and subsequent testing of mechanical strength and skin penetration could be performed using blank resin, without drug loading. Furthermore, as seen in Fig. 7A and B, for this optimal combination (70% VP, 30% PEGDA), the recovery of AHP-3 was determined to be

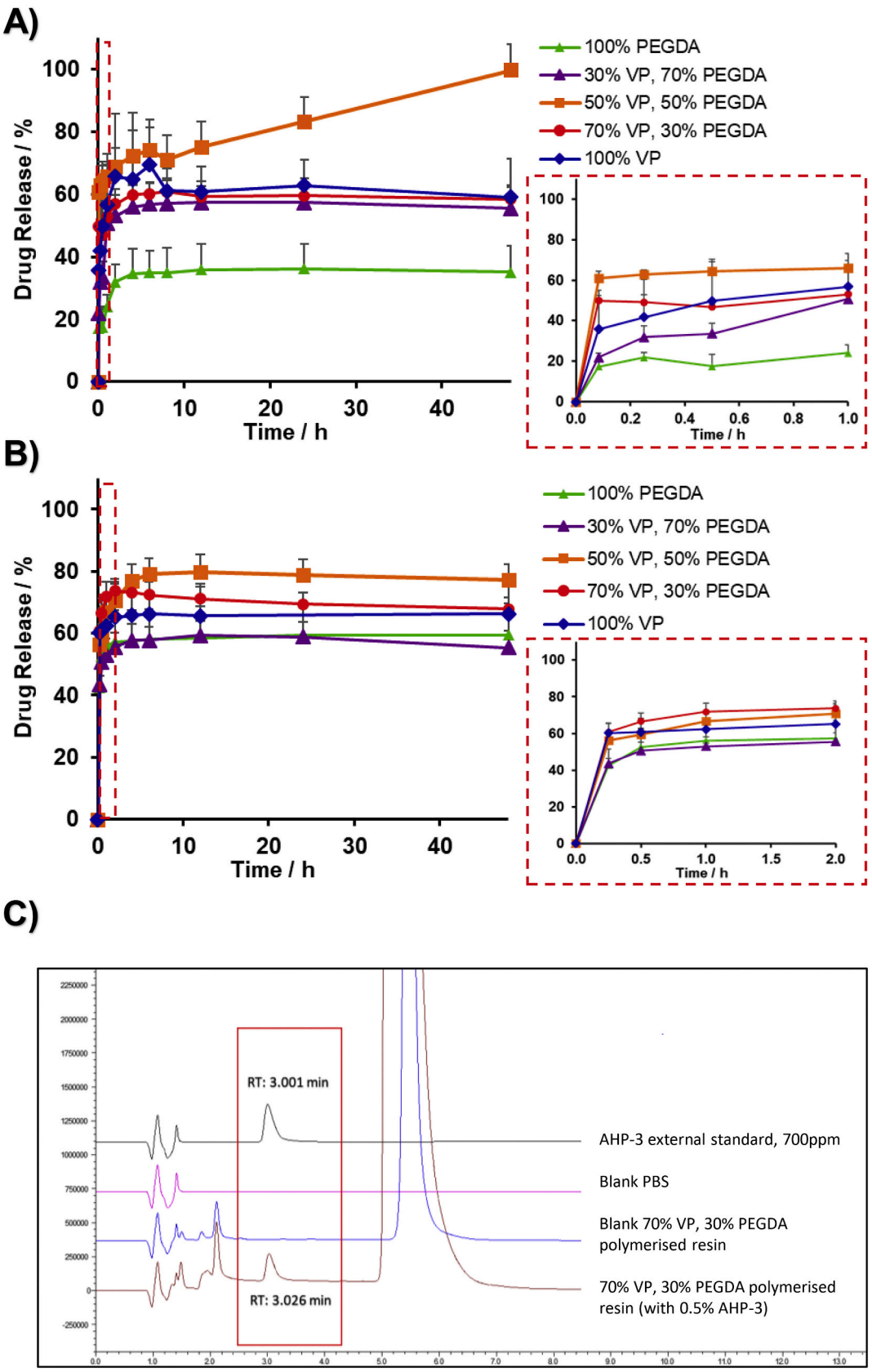

Fig. 7. Drug release study of various AHP-3 loaded cylinders. A) 0.1% w/w AHP-3 loaded cylinders; **B)** 0.5% *w*/w AHP-3 loaded cylinders; **C)** Sample HPLC Chromatogram. In both concentrations of AHP-3 loaded cylinders, 50% VP photopolymer cylinders consistently achieved the highest rate and overall drug release amongst all other photopolymers. On the other hand, 100% PEGDA consistently achieved the lowest rate and overall drug release amongst all other photopolymers. From the sample HPLC chromatogram, no changes to the retention of AHP-3 was observed in both the external standard and the polymerised resin. The experiments were performed in triplicates.

A)

	Young's Modulus (MPa)	
	Average	SD
70% VP, 30% PEGDA	29.12	4.51
70% VP, 30% PEGDA (With 0.5% AHP-3)	25.54	4.26

B)

	Time to 90% Polymerised /s	
	Average	S.D.
70% VP, 30% PEGDA	930.7	72.5
70% VP, 30% PEGDA (With 0.5% AHP-3)	985.7	18.5

Fig. 8. Physical properties and drug stability, after loading into optimised combination of VP and PEGDA. A) Young's modulus of drug loaded resin VS blank resin. B) Time to 90% polymerisation of drug loaded resin VS blank resin.

~70% for a 0.5% w/w AHP-3 loading and ~ 60% for a 0.1% w/w AHP-3 loading.

4.9. Design and fabrication of PMNP

Human volunteer face CAD model was used as a template to create a personalised patch as illustrated as red in Fig. 9A. This personalised patch was subsequently planted with arrays of MN in the geometry of a MN length 800 μm, tip diameter 100 μm, interspacing 800 μm and base diameter of 400 μm, as illustrated in Fig. 9B. The 3D-printed PMNP measures approximately 45 mm (length) x 30 mm (width) x 10 mm (height) with a total of 927 MNs embedded, as illustrated in Fig. 9C. Fig. 9D and E illustrates the microscope images of MN on the personalised surface. The average weight of each 3D printed microneedle patch was 2.668 g (± 0.034 g) with a printing time of approximately 1 h. After the patch was printed, it was soaked in 70%*v*/v ethanol in deionized water for 30 s, followed by pure deionized water for 30 s. The printed microneedle patch was finally post cured in the Asiga UV post cure chamber for an additional 30 min, before being used for any testing. AHP-3 peptide was also incorporated into the PMNP. This was achieved by mixing the pre-polymer solution with the AHP-3 peptide at a concentration of 0.5% *w*/w. Due to the nature of incorporation, AHP-3 peptide was present evenly in the entire patch.

4.10. Efficacy and safety of PMNP

Both skin penetration and mechanical strength are important predictors of MN efficacy. In Fig. 10A, trypan blue, which is a selective staining dye for hydrophilic surfaces, was employed to determine the presence of punctured pores within the epidermis. The blue dots as seen from the surface of the skin represented the punctured pores and therefore, the successful penetration of MNs through the human cadaver dermatomed skin. As illustrated in Fig. 10B, PMNP has over 98% of the MNs remaining intact after compression. This demonstrated a good mechanical strength and is less likely for any broken MN to be left within the skin resulting in complications. Previous cytotoxicity assays were performed on cylindrical rods fabricated using a PDMS mould. Here, we tested the whole 3D printing process, with the exact same parameters used for 3D printing PMNP, to 3D print several cubes of 5 mm each side. The resulting relative cell viability, as illustrated in Fig. 10C, demonstrated good biocompatibility of the optimised resin cube and the 3D printing process on HDF, with more than 80% of the cells surviving after a 24 h exposure.

5. Discussion

In this study, ratios of 2 commonly used liquid monomers of biocompatible polymers (PEGDA and PVP) were chosen as the starting point of optimisation. Both PEGDA and PVP were used frequently as a low toxicity, inert and biocompatible excipient in numerous oral and ophthalmic formulations [36] or even other microneedle applications [37,38]. However, while strong, PVP is brittle [39] and its monomer VP has very slow reactivity rate towards photo-polymerisation, as illustrated by 100% VP in Fig. 3A, and hence not suitable for 3D printing of biocompatible medical devices. PEGDA, on the other hand, has a very

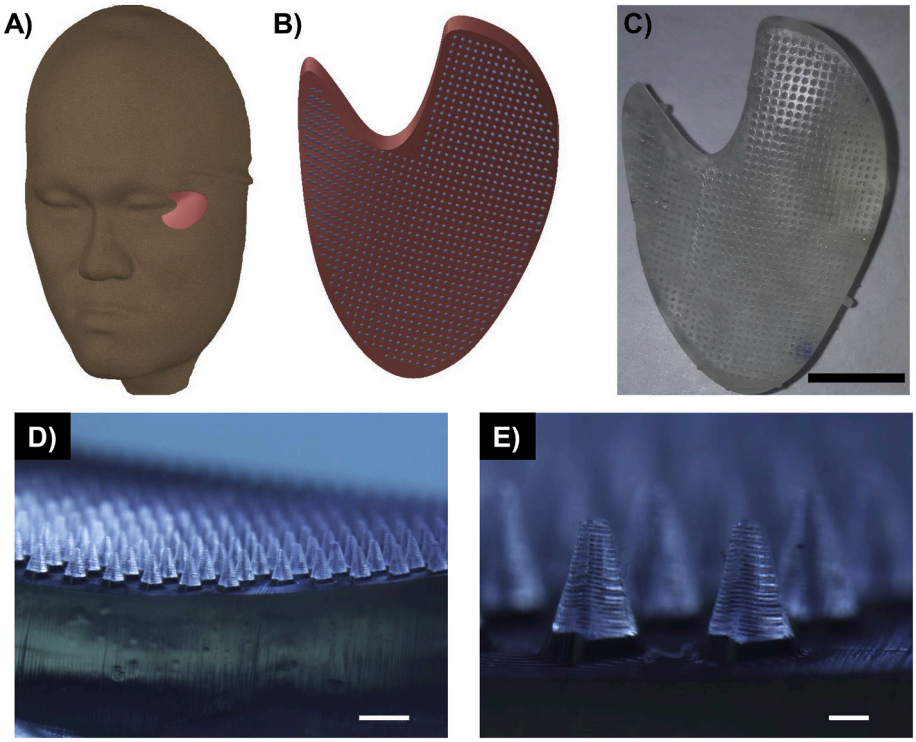

Fig. 9. CAD design and actual images of 3D printed personalised MN patch using optimised resin. A) 3D CAD model of human volunteer with eye patch contouring to the periorbital region; **B)** CAD model of personalised MN patch; **C)** 3D printed personalised MN patch (scalebar = 1 cm); **D)** Microscope image of personalised MN patch (scalebar = 1 mm); **E)** Zoomed in microscope image of personalised MN patch (scalebar = 200 μm).

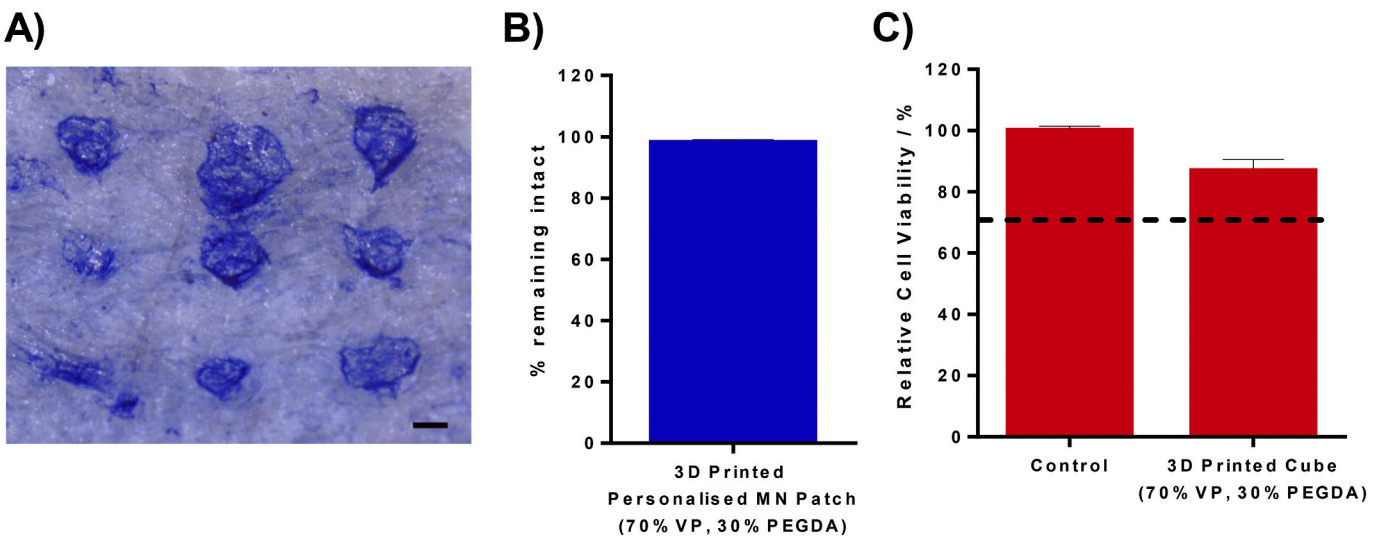

Fig. 10. Efficacy and safety parameters for 3D printed personalised MN patch. A) Skin penetration testing using trypan blue staining (scalebar = 200 μm), with the stained blue dots representing the punctured pores; B) Mechanical strength testing of 3D printed patch, with more than 95% of MN remaining intact after compression; C) Cytotoxicity essay for 3D printed cubes using same parameters as that of MN patch demonstrates good safety profile. The experiment was performed in triplicates. (For interpretation of the references to colour in this figure legend, the reader is referred to the web version of this article.)

fast reactivity rate, as illustrated by 100% PEGDA in Fig. 3A, towards photo-polymerisation. It also has a slight ductile nature [40] to its polymer but is not as strong as PVP, as illustrated by the Young's Modulus in Fig. 4B. By using both monomers together in a single 3D printable photopolymer resin, we have demonstrated an improved optimised resin to have a similar mechanical strength, with reduced brittleness, as compared to pure PVP and yet with improved reactivity rate, suitable for 3D printing. The optimised resin contained 7:3 ratio of VP:PEGDA. Using this optimised resin, we have also demonstrated the successful fabrication of high resolution PMNP that was able to penetrate the skin, possessed high mechanical strength and had minimal cytotoxicity to human dermal fibroblast cell lines.

Both PEGDA and VP undergoes free radical photo-polymerisation due to photoinitiator activation via UV–Vis light source. Generally, the higher the percentage of PEGDA (due to the presence of reactive acrylate group as compared to VP), the faster the rate of polymerisation, with the exception of 3:7 (VP:PEGDA) compared to pure PEGDA. This may be explained by the proposed hypothesis of autoacceleration caused by VP on acrylate polymerisation due to favourable hetero-polymerisation kinetics [41] and the reduced inhibition of acrylate polymerisation by oxygen [42].

On the other hand, White et al., demonstrated that with increasing concentration of VP above 30%, there is a decrease in mechanical strength of the resultant VP and acrylate copolymer, as compared to pure acrylate. This is similar to our study when the Young's Modulus of 3:7 (VP:PEGDA) is lower than that of pure PEGDA. However, in this study, we demonstrated the opposite trend where the higher the percentage of VP (above 50%), the higher the resultant Young's Modulus. This may be due to a separate 2 stage polymerisation as seen in Fig. 3A, where the more reactive acrylates will possibly react first followed by the less reactive VP group. Therefore, the optimised resin of 7:3 (VP:PEGDA) has a faster polymerisation rate compared to pure VP, and also a higher mechanical strength as compared to pure PEGDA.

In addition, by using different compositions of 2 monomers, we demonstrated the ability to control the swelling rate of polymers in Fig. 5. PVP has been known to be highly soluble in water and used to fabricate dissolvable MN [43]. However, when mixed with PEGDA, the resultant polymer was not water soluble, but instead swelled upon contact with water. A higher percentage of VP resulted in a higher swelling rate, which correlates to the rate and extent of drug release. Within 6 h, all the polymers reached its maximum extent of swelling. This implied that the maximum extent of drug release would have been achieved in 6 h. As demonstrated by McAvoy et al. [44], increased swelling after immersing in water for PEGDA 700 was correlated to an increased rate of drug release, as compared with PEGDA 250. This increased swelling was due to the reduced cross link density in PEGDA 700 (as compared with PEGDA 250). The reduced cross-linking density allowed more water ingression into the system and also the creation of more pores in the system, thus providing a higher rate of drug release. Interestingly, in this study, the rate of swelling did not correlate entirely with the rate of drug release. All VP containing photopolymers, as compared to 100% PEGDA, achieved a faster rate. However, comparing within the VP containing photopolymers only, the 50% VP photopolymer had consistently the highest rate of release, instead of the 70% VP photopolymer, which had the fastest rate of swelling. This could be due to the equal proportions of VP and PEGDA that resulted in a favourable crosslinked network that facilitates drug encapsulation and the subsequent release.

For the remaining VP compositions, there were no clear differences between their rate of drug release. When concentration of AHP-3 increased from 0.1% to 0.5%, there seemed to be a general increase in overall drug release. This could be due to the solubility of AHP-3 within the photopolymer combinations. Small fine particles of AHP-3 were oberved within the pre-polymer resin instead of completely being dissolved. This could mean that they were not incorporated within the polymer network and so, could be released quickly upon contact with PBS. Regardless, the control of drug release likely involved more than a single factor such as swelling rate of polymer and therefore requires more study to conclude.

Typically, the key components of a commercial photopolymer resin consist of the basic building monomers/oligomers, photoinitiator and light blocker to improve printing resolution. However, in this study, there was no addition of light blocker. By controlling the exposure time and separation distance of the build platform from resin container to allow fresh influx of resin, we were able to maintain the printing resolution. Furthermore, a yellow tint in the resultant resin due to BAPO could have contributed to a slight light blocking effect. The final printed part after post curing is clear in colour and therefore can also serve as a simple indicator to the user that most, if not all, of the photoinitiators had been utilised.

The dimensions of our microneedles were 800 μm in length, 100 μm in tip diameter, 800 μm for needle to needle interspacing and 400 μm in

base diameter. For microneedle tip, shaper tips can reduce the insertion force, but it may result in needle damage during skin insertion process, so a balance between sharpness of the tip and needle mechanical should be considered [45]. As demonstrated by Kochhar et al., even though the tip diameter is larger than 100 μm, the microneedle patch was still able to achieve skin penetration [34]. In another study, it has been found that blunt tips perform better to enhance skin permeability than sharp needles [46]. For the skin penetration testing here, the PMNP was inserted all at once, as an entire patch, using an average human thumb force of ~20 N. It has been reported that insertion force of microneedles with tip diameters ranging from 60 to 160 μm, ranged from 0.08 to 3.04 N [21].

The focus of this study is primarily to investigate the influence of the different ratios of two materials on the mechanical strength of the microneedles and the suitability for incorporation of a small peptide. In future experiments, the addition of adhesive materials could be considered to increase adhesion of the microneedle patch to the skin. Existing papers have shown that the microneedles after drug loading can be inserted into the skin without adding any adhesives. Previous studies relating to microneedle patches used materials such as polyethylene glycol diacrylate (PEGDA) and polyvinylpyrrolidone (PVP), similar to those in this current study. For example, Tas et al. used PVP to carry the drug dihydroergotamine methanesulfonate to make a microneedle patch for treatment of migraines without using sticky materials [37]. In another example, adhesives such as scotch tapes could also be fixed to the microneedle patch after fabrication. Kathuria et al. demonstrated the use of a microneedle patch made of lidocaine mixed within PEGDA [38]. The large size microneedle patch was successfully adhered to the porcine body using scotch tape attached onto the back of the fabricated microneedle patch.

Any residual monomers could be removed by immersing PMNP in PBS or water for an extended period of time. In our study, using ^{1}H NMR, we have shown that the resin was almost 100% polymerised. Therefore, only minimal post processing was required. This was further confirmed by the in vitro toxicity study with human dermal cell lines. In addition, extended period of immersing PMNP in PBS or water could remove the embedded AHP-3 which would make the final dose inconsistent. Therefore, we believe that our current post processing procedure would be the most optimised method to balance the efficacy and safety aspects of the PMNP. Based on FDA guidelines on Biological evaluation of medical devices [47], the recommended test for medical devices to be used on intact skin include cytotoxicity, sensitisation and irritation or intracutaneous reactivity. Therefore, for PMNP or even the new optimised polymer, there will be a need for a minimal of these 3 tests, before it can be truly considered biocompatible for microneedle transdermal drug delivery.

Due to the nature of incorporation, AHP-3 peptide was present evenly in the patch. This way of incorporation could be a fast and convenient means of incorporating active ingredients into microneedle patch as illustrated by Kochhar et al. [48]. Furthermore, the presence of AHP-3 peptide in the patch served as a drug reservoir for sustained delivery of AHP-3 and provided an avenue for higher drug loading. The average weight of the printed microneedle patch was 2.668 g (±0.034 g). Therefore, the average amount of AHP-3 peptide incorporated in each patch was ~13 mg. AHP-3 peptides are potent, and the amount required for antiwrinkle effect is less as compared to chemical drugs. From previous study by Lim et al. [8], approximately 0.8 mg (or 2 mM solution) of AHP-3 peptide was required to reduce the amount of glutamate release in neuron cell (as a surrogate marker for an increase in antiwrinkle effect). Furthermore, a mean wrinkle reduction of 16.26% was also achieved in a clinical study using 0.05% cream formulation twice a day for 28 days [49].

In this study, it was demonstrated that AHP-3 was stable in the base polymer material after photo-crosslinking and could be released when immersed in PBS. Further studies need to be performed to determine the actual release profile of AHP-3 from the PMNP. However, based on previous studies, the AHP-3 could be estimated to have a burst release at the start, before achieving a slower steady state of release subsequently. As demonstrated by Lim et al. [30], compared with a solution of AHP-3 and intact skin, transdermal delivery of AHP-3 could be enhanced with microneedle pre-treatment, up to 90-fold higher. In our study, the incorporation of AHP-3 in the PMNP provide a standardized dosing and could be a convenient single-step procedure for the user self-administration. Furthermore, our PMNP could also provide a sustained release of AHP-3 as the base material swells in contact with fluids and releases the incorporated AHP-3 over time.

Pliable or flexible microneedle patches could potentially allow the microneedles to adhere closely to the human skin instead of the need for a 3D printed personalised microneedle patch. However, as discussed by Lim et al. [29], these flexible microneedle patches would likely require a degree of user expertise for proper application, to ensure no embedded air pockets or uneven adherence to the skin. Furthermore, these microneedle patches may not be of sufficient flexibility to account for the minor indentations or variations of the skin. Finally, the process of 3D scanning of patient's face could be automated and is relatively quick (approximately a few minutes). Therefore, the amount of time taken, as compared to the fabrication duration of 3D printing, would be insignificant.

To our best knowledge, this is the first study that investigated the combination of VP and PEGDA for its use in 3D printing of drug delivery application. Commercially available resins are not suitable for drug delivery application due to their inability to embed drugs within and release the drugs subsequently. Furthermore, we have also demonstrated the that the loading of AHP-3 within the resin and subsequently polymerisation, has no detrimental effect on the stability of AHP-3 as a small peptide. This meant that the optimised resin and the 3D printing process may also be used for other peptides of therapeutic effects. The use of handheld 3D scanners and CAD software also demonstrated a convenience in developing PMNP which have potential to be used in drug delivery applications for other regions of the body such as scalp for hair loss or joints for pain relief. Future applications such as wearable devices for smart delivery of drugs or bio-sensing may also be possible.

6. Conclusion

Physical characterisation of 3D printable, high resolution photopolymer resin was conducted. Based on these results, an optimised photopolymer resin of 7:3 (VP: PEGDA) was developed, with adequate mechanical strength, reasonable polymerisation time and minimal cytotoxicity. High resolution 3D printing of PMNP was achieved using the optimised resin. Subsequently, in vitro characterisation of the fabricated PMNP also demonstrated the ability to penetration skin and to remain intact after compression. Together, with increased knowledge on photopolymer optimisation, the advancements in 3DP technology and availability of software such as Materialize Mimics® which enables conversion of medical imaging scans to CAD models, 3D printing may provide a viable approach for PMNP fabrication to enhance transdermal delivery of AHP-3 for anti-wrinkle therapy in the future.

Funding

Singapore National Additive Manufacturing Innovation Cluster (NAMIC) project 2016011 and Singapore MOE AcRF Tier 1 grant (R148-000-224-112).

Credit authorship contribution statement

Seng Han Lim: Conceptualization, Methodology, Investigation, Writing - original draft, Writing - review & editing. **Himanshu Kathuria**: Methodology, Investigation, Writing - review & editing, Writing - original draft. **Muhd Hafiz Bin Amir**: Methodology, Investigation, Writing - original draft. **Xiyuan Zhang**: Writing - review & editing. **Hien T.T. Duong**: Writing - review & editing. **Paul Chi-Lui Ho**: Resources,

Supervision, Writing - review & editing. **Lifeng Kang**: Conceptualization, Methodology, Writing - review & editing, Supervision, Funding acquisition, Project administration.

Declaration of competing interest

There is no conflict of interest for all authors.

Appendix A. Supplementary data

Supplementary data to this article can be found online at https://doi.org/10.1016/j.jconrel.2020.10.021.

References

[1] J.J. Manriquez, D. Majerson Gringberg, C. Nicklas Diaz, Wrinkles, BMJ Clin. Evid. 2008 (2008) 1711.
[2] R. Ganceviciene, A.I. Liakou, A. Theodoridis, E. Makrantonaki, C.C. Zouboulis, Skin anti-aging strategies, Dermatoendocrinol 4 (2012) 308–319.
[3] M. Gupta, A. Gupta, Photodamaged skin and quality of life: reasons for therapy, J. Dermatol. Treat. 7 (1996) 261–264.
[4] ASAPS, Cosmetic Surgery National Data Bank: Procedural Statistics (the American Society for Aesthetic Plastic Surgery). https://www.surgery.org/sites/default/files/ASAPS-Stats2017.pdf.
[5] A.V. Benedetto, The environment and skin aging, Clin. Dermatol. 16 (1998) 129–139.
[6] C. Blanes-Mira, J. Clemente, G. Jodas, A. Gil, G. Fernandez-Ballester, B. Ponsati, L. Gutierrez, E. Perez-Paya, A. Ferrer-Montiel, A synthetic hexapeptide (Argireline) with antiwrinkle activity, Int. J. Cosmet. Sci. 24 (2002) 303–310.
[7] P.S. Yamauchi, N.J. Lowe, Botulinum toxin types A and B: comparison of efficacy, duration, and dose-ranging studies for the treatment of facial rhytides and hyperhidrosis, Clin. Dermatol. 22 (2004) 34–39.
[8] S.H. Lim, Y. Sun, T. Thiruvallur Madanagopal, V. Rosa, L. Kang, Enhanced skin permeation of anti-wrinkle peptides via molecular modification, Sci. Rep. 8 (2018) 1596.
[9] M.P. Lupo, A.L. Cole, Cosmeceutical peptides, Dermatol. Ther. 20 (2007) 343–349.
[10] Y. Wang, M. Wang, S. Xiao, P. Pan, P. Li, J. Huo, The anti-wrinkle efficacy of argireline, a synthetic hexapeptide, in Chinese subjects: a randomized, placebo-controlled study, Am. J. Clin. Dermatol. 14 (2013) 147–153.
[11] M.E. Kraeling, W. Zhou, P. Wang, O.A. Ogunsola, In vitro skin penetration of acetyl hexapeptide-8 from a cosmetic formulation, Cutan. Ocul. Toxicol. 34 (2015) 46–52.
[12] M. Hoppel, G. Reznicek, H. Kahlig, H. Kotisch, G.P. Resch, C. Valenta, Topical delivery of acetyl hexapeptide-8 from different emulsions: influence of emulsion composition and internal structure, Eur. J. Pharm. Sci. 68 (2015) 27–35.
[13] M.A. Ruiz, B. Clares, M.E. Morales, S. Cazalla, V. Gallardo, Preparation and stability of cosmetic formulations with an anti-aging peptide, Int. J. Cosmet. Sci. 58 (2007) 157–171.
[14] E. Larraneta, J. Moore, E.M. Vicente-Perez, P. Gonzalez-Vazquez, R. Lutton, A. D. Woolfson, R.F. Donnelly, A proposed model membrane and test method for microneedle insertion studies, Int. J. Pharm. 472 (2014) 65–73.
[15] K. van der Maaden, W. Jiskoot, J. Bouwstra, Microneedle technologies for (trans) dermal drug and vaccine delivery, J. Control. Release 161 (2012) 645–655.
[16] L.Y. Chu, S.O. Choi, M.R. Prausnitz, Fabrication of dissolving polymer microneedles for controlled drug encapsulation and delivery: bubble and pedestal microneedle designs, J. Pharm. Sci. 99 (2010) 4228–4238.
[17] J.S. Kochhar, P. Anbalagan, S.B. Shelar, J.K. Neo, C. Iliescu, L. Kang, Direct microneedle array fabrication off a photomask to deliver collagen through skin, Pharm. Res. 31 (2014) 1724–1734.
[18] J.S. Kochhar, W.X. Lim, S. Zou, W.Y. Foo, J. Pan, L. Kang, Microneedle integrated transdermal patch for fast onset and sustained delivery of lidocaine, Mol. Pharm. 10 (2013) 4272–4280.
[19] K. Ita, Transdermal delivery of drugs with microneedles-potential and challenges, Pharmaceutics 7 (2015) 90–105.
[20] S.F. Lahiji, M. Dangol, H. Jung, A patchless dissolving microneedle delivery system enabling rapid and efficient transdermal drug delivery, Sci. Rep. 5 (2015) 7914.
[21] S.P. Davis, B.J. Landis, Z.H. Adams, M.G. Allen, M.R. Prausnitz, Insertion of microneedles into skin: measurement and prediction of insertion force and needle fracture force, J. Biomech. 37 (2004) 1155–1163.
[22] A. Vrdoljak, M.G. McGrath, J.B. Carey, S.J. Draper, A.V.S. Hill, C. O'Mahony, A. M. Crean, A.C. Moore, Coated microneedle arrays for transcutaneous delivery of live virus vaccines, J. Control. Release 159 (2012) 34–42.
[23] E.S. Esser, J.A. Pulit-Penaloza, H. Kalluri, D. McAllister, E.V. Vassilieva, E. Q. Littauer, N. Lelutiu, M.R. Prausnitz, R.W. Compans, I. Skountzou, Microneedle patch delivery of influenza vaccine during pregnancy enhances maternal immune responses promoting survival and long-lasting passive immunity to offspring, Sci. Rep. 7 (2017) 5705.
[24] E. Jacoby, C. Jarrahian, H.F. Hull, D. Zehrung, Opportunities and challenges in delivering influenza vaccine by microneedle patch, Vaccine 33 (2015) 4699–4704.
[25] K.A. Moga, L.R. Bickford, R.D. Geil, S.S. Dunn, A.A. Pandya, Y. Wang, J.H. Fain, C. F. Archuleta, A.T. O'Neill, J.M. Desimone, Rapidly-dissolvable microneedle patches via a highly scalable and reproducible soft lithography approach, Adv. Mater. 25 (2013) 5060–5066.
[26] B. Cai, W. Xia, S. Bredenberg, H. Li, H. Engqvist, Bioceramic microneedles with flexible and self-swelling substrate, Eur. J. Pharm. Biopharm. 94 (2015) 404–410.
[27] C.K. Choi, J.B. Kim, E.H. Jang, Y.N. Youn, W.H. Ryu, Curved biodegradable microneedles for vascular drug delivery, Small 8 (2012) 2483–2488.
[28] M. Kim, T. Kim, D.S. Kim, W.K. Chung, Curved microneedle array-based sEMG electrode for robust long-term measurements and high selectivity, Sensors 15 (2015) 16265–16280.
[29] S.H. Lim, J.Y. Ng, L. Kang, Three-dimensional printing of a microneedle array on personalized curved surfaces for dual-pronged treatment of trigger finger, Biofabrication 9 (2017), 015010.
[30] S.H. Lim, W.J. Tiew, J. Zhang, P.C. Ho, N.N. Kachouie, L. Kang, Geometrical optimisation of a personalised microneedle eye patch for transdermal delivery of anti-wrinkle small peptide, Biofabrication 12 (2020) 035003.
[31] C.J. Bloomquist, M.B. Mecham, M.D. Paradzinsky, R. Janusziewicz, S.B. Warner, J. C. Luft, S.J. Mecham, A.Z. Wang, J.M. DeSimone, Controlling release from 3D printed medical devices using CLIP and drug-loaded liquid resins, J. Control. Release 278 (2018) 9–23.
[32] H.M. Mansour, M. Sohn, A. Al-Ghananeem, P.P. Deluca, Materials for pharmaceutical dosage forms: molecular pharmaceutics and controlled release drug delivery aspects, Int. J. Mol. Sci. 11 (2010) 3298–3322.
[33] S. Liu, D.C. Yeo, C. Wiraja, H.L. Tey, M. Mrksich, C. Xu, Peptide delivery with poly (ethylene glycol) diacrylate microneedles through swelling effect, Bioeng. Transl. Med. 2 (2017) 258–267.
[34] J.S. Kochhar, T.C. Quek, W.J. Soon, J. Choi, S. Zou, L. Kang, Effect of microneedle geometry and supporting substrate on microneedle array penetration into skin, J. Pharm. Sci. 102 (2013) 4100–4108.
[35] M.B. Huglin, K.S. Khairou, Copolymerisations of N-vinyl pyrrolidone with styrene and n-butyl acrylate, Eur. Polym. J. 24 (1988) 239–243.
[36] P. Ronnander, L. Simon, H. Spilgies, A. Koch, S. Scherr, Dissolving polyvinylpyrrolidone-based microneedle systems for in-vitro delivery of sumatriptan succinate, Eur. J. Pharm. Sci. 114 (2018) 84–92.
[37] C. Tas, J.C. Joyce, H.X. Nguyen, P. Eangoor, J.S. Knaack, A.K. Banga, M. R. Prausnitz, Dihydroergotamine mesylate-loaded dissolving microneedle patch made of polyvinylpyrrolidone for management of acute migraine therapy, J. Control. Release 268 (2017) 159–165.
[38] H. Kathuria, H. Li, J. Pan, S.H. Lim, J.S. Kochhar, C. Wu, L. Kang, Large size microneedle patch to deliver lidocaine through skin, Pharm. Res. 33 (2016) 2653–2667.
[39] C. Liu, C. Xiao, H. Liang, Properties and structure of PVP–lignin "blend films", J. Appl. Polym. Sci. 95 (2005) 1405–1411.
[40] S. Hong, D. Sycks, H.F. Chan, S. Lin, G.P. Lopez, F. Guilak, K.W. Leong, X. Zhao, 3D printing of highly stretchable and tough hydrogels into complex, cellularized structures, Adv. Mater. 27 (2015) 4035–4040.
[41] J. White Timothy, B. Liechty William, C.A. Guymon, The influence of N-vinyl pyrrolidone on polymerization kinetics and thermo-mechanical properties of crosslinked acrylate polymers, J. Polym. Sci. A Polym. Chem. 45 (2007) 4062–4073.
[42] D.H. Lorenz, J.L. Azorlosa, R.S. Tu, N-vinyl-2-pyrrolidone as a reactive diluent in radiation curing, Radiat. Phys. Chem. 9 (1977) 843–849.
[43] Y.J. Juang, Y.L. Deng, I.C. Lee, Membrane filtration: an unconventional route for fabrication of the flexible and dissolvable, polymer microneedle patches, Biomicrofluidics 10 (2016), 044108.
[44] K. McAvoy, D. Jones, R.R.S. Thakur, Synthesis and characterisation of photocrosslinked poly(ethylene glycol) diacrylate implants for sustained ocular drug delivery, Pharm. Res. 35 (2018) 36.
[45] G. Ma, C. Wu, Microneedle, bio-microneedle and bio-inspired microneedle: a review, J. Control. Release 251 (2017) 11–23.
[46] W.Z. Li, M.R. Huo, J.P. Zhou, Y.Q. Zhou, B.H. Hao, T. Liu, Y. Zhang, Super-short solid silicon microneedles for transdermal drug delivery applications, Int. J. Pharm. 389 (2010) 122–129.
[47] FDA, Guidance Documents (Medical Devices and Radiation-Emitting Products). https://www.fda.gov/downloads/medicaldevices/deviceregulationandguidance/guidancedocuments/ucm348890.pdf.
[48] J.S. Kochhar, W.J. Goh, S.Y. Chan, L. Kang, A simple method of microneedle array fabrication for transdermal drug delivery, Drug Dev. Ind. Pharm. 39 (2013) 299–309.
[49] F. Gorouhi, H.I. Maibach, Role of topical peptides in preventing or treating aged skin, Int. J. Cosmet. Sci. 31 (2009) 327–345.